Ni introduction induced non-radical degradation of bisphenol A in spinel ferrites/H_2O_2 systems

Yilan Jiang, Keyi Gao, Yingying Li, Yuanyuan Chen, Xingyang Cai, Dawei Wang[a,*]

Key Laboratory of Integrated Regulation and Resource Development on Shallow Lake of Ministry of Education, College of Environment, Hohai University, Nanjing 210098, P. R. China

D.W.: dawei.wang@hhu.edu.cn

Number of pages: 22

Number of Text: 6

Number of Figures: 15

Number of Tables: 3

Contents

Text

Figures

Tables

Text S1. Materials

Ferric nitrate nonahydrate ($Fe(NO_3)_3·9H_2O$, > 98.5%), nickel nitrate hexahydrate ($Ni(NO_3)_2·6H_2O$, 99%), cobalt nitrate hexahydrate ($Co(NO_3)_2·6H_2O$, 98.5%), sodium hydroxide (NaOH, 96%), hydrogen peroxide (H_2O_2, 30%), sodium sulfite (Na_2SO_3, 97%), potassium chloride (KCl, 99.5%), potassium nitrate (KNO_3, 99%), potassium dihydrogen phosphate (KH_2PO_4, 99%), isopropyl alcohol (IPA, 99.7%), phosphoric acid (H_3PO_4, 85%), and ferrous sulfate heptahydrate ($FeSO_4·7H_2O$, > 98.5%) were purchased from Sinopharm Chemical Reagent Co., Ltd.; BPA (99%) was purchased from Shanghai Yuanye Bio-Technology Co., Ltd.; HA (90%), furfuryl alcohol (FFA, 97%) and benzoic acid (BA, 99.5%) were purchased from Shanghai Aladdin Biochemical Technology Co., Ltd.; *p*-benzoquinone (*p*-BQ, 99 %) was purchased from Shanghai Macklin Biochemical Technology Co., Ltd.; L-histidine (*L*-his, chromatographic purity) was purchased from Shanghai Huixing Biochemical Technology Co., Ltd.; Methanol (≥99.9%) was purchased from Merck KGaA. Hydrochloric acid (HCl, 36~38%) was purchased from Shanghai Lingfeng Chemical Reagent Co., Ltd. And 5,5-dimethyl-1-pyrroline N-oxide (DMPO) were purchased from DOJINDO Laboratories. 2,2,6,6-tetramethyl-4-piperidinol (TEMP) was purchased from Nanjing Lisheng Kanghe Biotechnology Co., Ltd. All the chemicals were used without further purification.

Text S2. The preparation and characterization methods of catalysts

$Co_{1-x}Ni_xFe_2O_4$ (x= 0, 0.5, 1) catalysts were prepared by a hydrothermal method. Firstly, $Co(NO_3)_3·6H_2O$, $Fe(NO_3)_3·9H_2O$, and $Ni(NO_3)_3·6H_2O$ with a certain stoichiometric ratio were dissolved in 20 mL deionized water under magnetic stirring. Detailed dosing amounts of precursors for different $Co_{1-x}Ni_xFe_2O_4$ catalysts are listed in the supplementary information (Table S1). Then, 20 mL of 2 M KOH was added. After stirring for 1 h, the homogeneous solution was transferred into a 100 mL sealed Teflon-lined autoclave and kept at 160 °C for 10 h. The precipitate was washed with distilled water and centrifuged several times. Eventually, the sample was dried at 60 ^oC for 12 h.

Text S3. Characterization

X-ray diffraction (XRD) measurements were performed with a Rigaku Ultima IV (Cu Ka radiation, λ = 1.5406 Å) in the range of 20°−80° and at a scanning rate of 4°/min to evaluate phase purity and analyze crystal structure. X-ray photoelectron spectroscopy (XPS) was used to obtain the surface composition and electronic structure, which were recorded with an ESCALAB 250Xi electron energy spectrometer, using Al Kα (1486.6 eV) as the X-ray excitation source. Scanning electron microscopy (SEM) was used to observe the micro morphology of materials. Transmission electron microscopy (TEM) and high-resolution TEM (HRTEM) analysis of these samples were characterized using a Tecnai G2 F20 with an accelerating voltage of 200 kV. The concentration of pollutants was determined by a high performance liquid chromatograph (HPLC, Agilent 1200) equipped with a C18 reversed phase column (4.6 mm × 150 mm). Electron paramagnetic resonance (EPR) spectrometer (Magnettech ESR5000, Bruker) was employed to detect the active species. Identification of intermediates using ultra-high performance liquid chromatography-mass spectrometry (HPLC-MS).

Text S4. Determination of degradation process

The degradation experiments were carried out in 100 mL beaker with 50 mL of BPA solution (0.1 mM). pH was 3.0 and H_2O_2 concentration was 20 mM and $Co_{1-x}Ni_xFe_2O_4$ concentration was 2.0 g/L. In a typical experiment, the $Co_{1-x}Ni_xFe_2O_4$ was added into the BPA solution and the pH was adjusted, under stirring for 30 min to reach adsorption equilibrium. Afterward, a certain amount of H_2O_2 was quickly spiked to initiate the reaction. Aliquots of the solution was sampled at set time interval. To quench the possible reactions from excessing amount of H_2O_2, 20 μL of 2 M Na_2SO_3 solution was immediately spiked into the samples, which was subsequently filtered with a 0.22 μm Teflon (PTFE) membrane filter and analyzed immediately with HPLC instrument (details of the conditions of the HPLC analysis are provided further below). The removal ratio of BPA was calculated by C/C_0, where C was the concentration of BPA at given time and C_0 was the initial concentration of BPA. To

test the interfering effects of water components, KCl, KNO_3, KH_2PO_4 (5 mM) or HA (50 mg/L) was added into the BPA solution, while other experimental parameters remained the same. pH was adjusted to 3.0 for these experiments.

The concentrations of BPA were measured by a high-performance liquid chromatography (HPLC) instrument. Methanol/deionized water (70:30 v/v) was used as the mobile phase and the wavelength was set at 280 nm. The injection volume was 20 μL and flow rate of mobile phase was 1 mL/min. The detection limit of BPA was 0.05 mg/L and 0.1 mg/L, respectively. The rate constant of the catalytic reactions followed the pseudo-first-order model as follows (Eq. 1):

$$ln\frac{C}{C_0} = -kt \quad (1)$$

where C (mg L^{-1}) is the target pollutant concentration, t (min) is the reaction time, and k (min^{-1}) is the pseudo-first-order rate constant.

Text S5. Identification of active species

Scavenging experiments of active species were performed as follows：A certain amount of $Co_{1-x}Ni_xFe_2O_4$ was added into the 0.1 mM BPA solution. Subsequently, scavengers of 100 mM IPA, 10 mM *p*-BQ, 10 mM *L*-his and 10 mM PMSO were separately added into the solution to probe $\cdot OH$, $\cdot O_2^-$, $^1O_2$ and high-valence metals (M_v), respectively [1, 2]. Then, the solution pH was adjusted to 3.0 using 2 M HCl. The subsequent steps were consistent with those experiments without any scavengers. The contribution rate of each active species (CR) was estimated by the following Eqs. [3]:

$$RC_{\cdot OH} = \frac{k_{\cdot OH}}{k_{app}} \approx \frac{k_{app} - k_{IPA}}{k_{app}} \quad (2)$$

$$RC_{\cdot O_2^-} = \frac{k_{\cdot O_2^-}}{k_{app}} \approx \frac{k_{app} - k_{p-BQ}}{k_{app}} \quad (3)$$

$$RC_{^1O_2} = \frac{k_{^1O_2}}{k_{app}} \approx \frac{k_{app} - k_{L-his}}{k_{app}} \quad (4)$$

$$RC\ Mv = \frac{k_{Mv}}{k_{app}} \approx \frac{k_{app} - k_{PMSO}}{k_{app}} \quad (5)$$

where *CR*, k_{app}, k_{IPA}, $k_{p\text{-}BQ}$, $k_{L\text{-}his}$ and k_{PMSO} represent the contribution rate percentage and the apparent rate constant for BPA degradation in the absence and in the presence of IPA, *p*-BQ, *L*-his and PMSO respectively.

Electron paramagnetic resonance (EPR) was used to further confirm ROS by reacting with DMPO and TEMP. The pH of DMPO and TEMP solution were both adjusted to 3.0 prior to use. One mL of sample was collected from the $NiFe_2O_4/H_2O_2$ reaction system (catalyst: 2 g/L, H_2O_2: 50 mM and pH: 3.0), then 100 μL of DMPO or TEMP solution were mixed with the samples before the measurement of spin-trapping adducts in the EPR instrument. To explore the source of $^1O_2$, 0.1 M of IPA or 0.01 M *p*-BQ solution was added as scavenging agents for ·OH and $\cdot O_2^-$ in the solution with TEMP. Spin-trapping adducts are measured before and after H_2O_2 addition under the pH was 3.0.

In addition, 0.1 mM FFA was employed as molecular probe to measure the amount of $^1O_2$ produced during the Fenton-like reaction. FFA concentrations were measured using HPLC: methanol/H_2O (50:50 v/v) was used as the mobile phase, and the detection wavelength was set at 219 nm.

To quantify the production of ·OH, a probe reaction was conducted by oxidizing BA to p-hydroxybenzoic acid (p-HBA). The concentration of BA was chosen as 10 mM, and the initial pH value of the solution was 3.0. The *p*-HBA was quantitatively analyzed using the HPLC and the mobile phase was a mixture of acetonitrile and 0.1% H_3PO_4 aqueous solution (35:65, v/v) at a flow rate of 1 mL/min, with the detection wavelength at 255 nm [4, 5].

cumulative OH• produced = [*p*-HBA] × 5.87 (6)

where [p-HBA] is the concentration of *p*-HBA (mol L^{-1}).

Text S6. Electrochemical tests

The electrochemical tests were conducted in a three-electrode system. A glassy carbon electrode loaded with catalysts was used as working electrodes, while

platinum wire electrode as counter electrodes and Ag/AgCl electrode as reference electrodes. First, 8 mg catalyst and 20 μL Nafion solution (5 wt.%) were dispersed in water/ethanol mixed solution (1 mL) under ultrasonication for 30 min. Then, 10 μL mixture was dropped onto the surface of polished glassy carbon electrode and dried at room temperature. The scanning rate in cyclic voltammetry (CV) tests was 200 mV. s^{-1} and the scanning direction is positive.

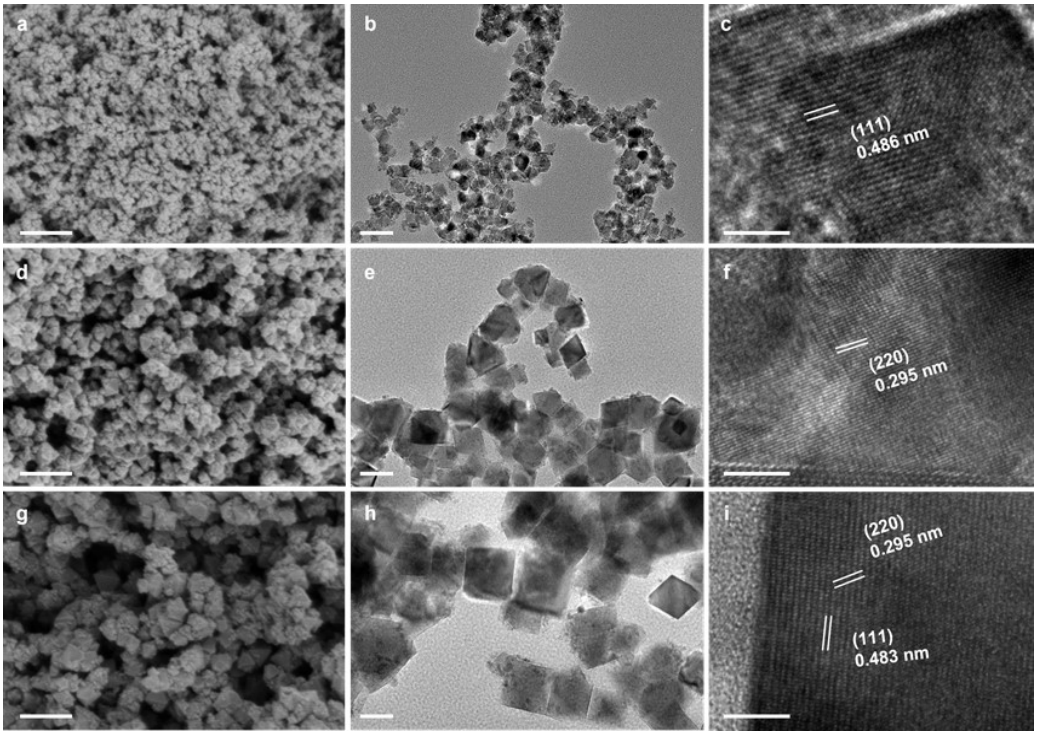

Fig. S1 SEM(a), TEM(b) and HRTEM images (c) of $CoFe_2O_4$; SEM(d), TEM(e) and HRTEM images (f) of $Co_{0.5}Ni_{0.5}Fe_2O_4$; SEM(g), TEM(h) and HRTEM images (i) of $NiFe_2O_4$; scale bars in SEM represent 250 nm; scale bars in TEM and HRTEM images represent 50 nm and 2 nm, respectively. The lattice fringes displayed interplanar spacing of 0.486 nm, which matched well with the (111) plane of $CoFe_2O_4$. For $Ni_{0.5}Co_{0.5}Fe_2O_4$, the HRTEM image presented a clear lattice distance of 0.295 nm, corresponding to the (220) plane. Moreover, the lattice fringes of $NiFe_2O_4$ displayed interplanar spacing of 0.295 nm and 0.483 nm, which matched well with the (220) and (111) plane, respectively.

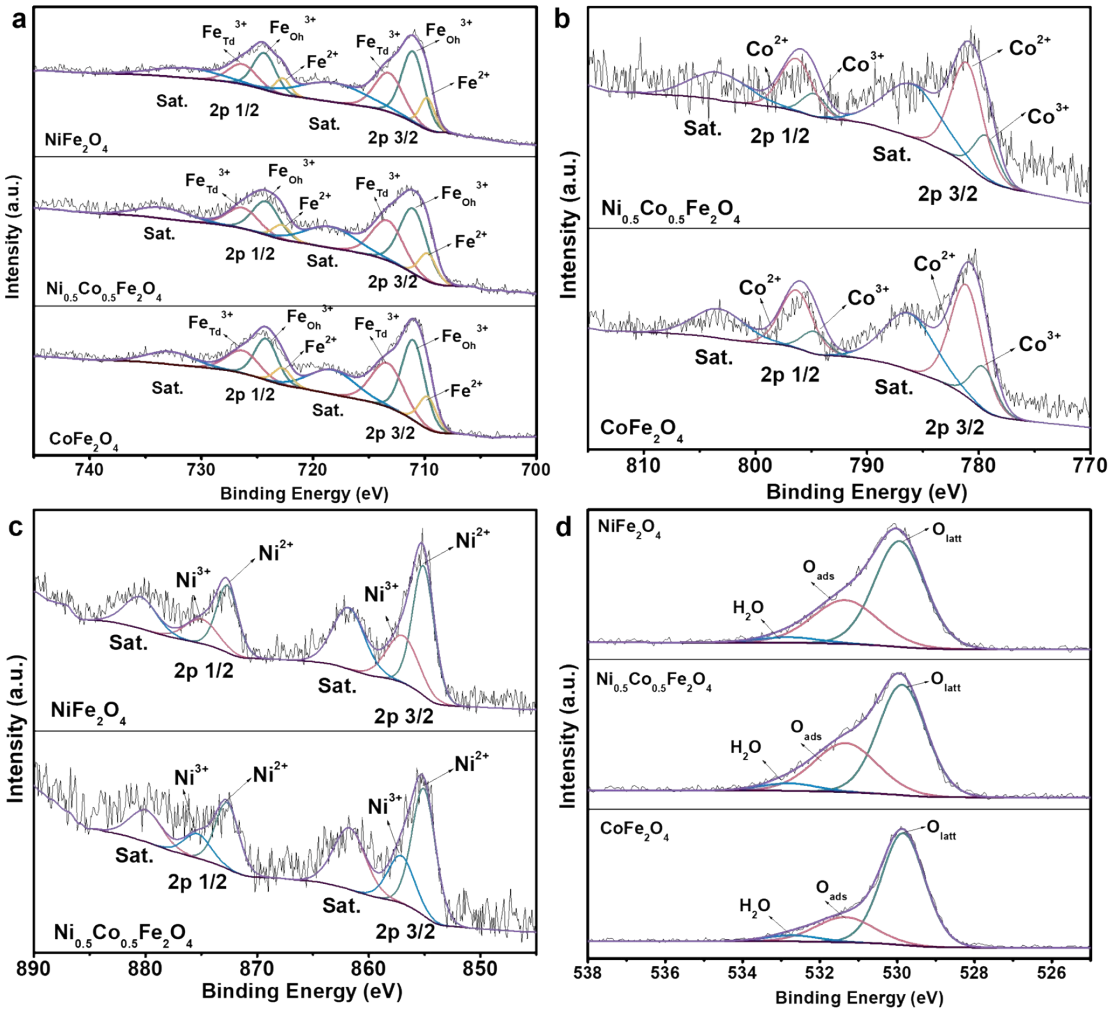

Fig. S2 (a) Fe 2p, (b) Ni 2p and (c) Co 2p XPS spectra for $CoFe_2O_4$, $Ni_{0.5}Co_{0.5}Fe_2O_4$ and $NiFe_2O_4$. Owing to the spin-orbit coupling, 2p spectra are split into 2p3/2 and 2p1/2 doublets along with two satellite peaks. The peaks at 709.7 and 722.6 eV corresponded to Fe^{2+} species, the peaks at 711.1 and 724.3 eV were assigned to Fe^{3+} species in Oh site while the peaks at 713.3 and 726.4 eV were assigned to Fe^{3+} species in Td site [6-8]. For Co 2p, the peaks at 781.4 and 796.3 eV were assigned to Co^{2+} species while the peaks at 779.4 and 794.8 eV were assigned to Co^{3+} species [6, 7]. Ni 2p also reveals the existence of two valence states, the peaks at 855.2 and 872.8 eV were assigned to Ni^{2+} species while the peaks at 857.1 and 875.1 eV were assigned to Ni^{3+} species [8]. The O 1s peaks of the samples can be fitted into three peaks, which were attributed to lattice oxygen (O_{latt}, 529.9 eV), surface absorbed oxygen (O_{ads}, 531.5 eV), and water molecules adsorbed on the surface (H_2O, 532.5 eV) [9, 10]. The

ratio of metal ion with different electronic structure and the proportions of O_{ads} are also listed in Table S2. As shown in Table S2, the values of $Fe_{Oh}^{3+}/Fe_{Td}^{3+}$ did not change significantly, indicating that after the introduction of Ni, most of the positions of Co were occupied by Ni, which is the octahedral position in the spinel lattice.

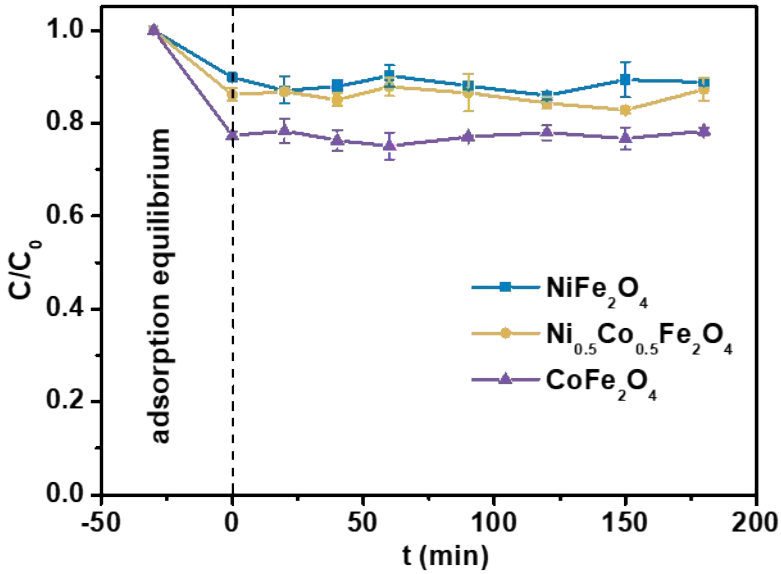

Fig. S3 BPA removal by catalyst adsorption. Different samples have different adsorption capacities for BPA, and the reason why $CoFe_2O_4$ adsorbed more BPA may be due to the smaller size and more adsorption sites. However, all samples reached adsorption equilibrium within 30 minutes, and the adsorption amount remained unchanged after further extension of time.

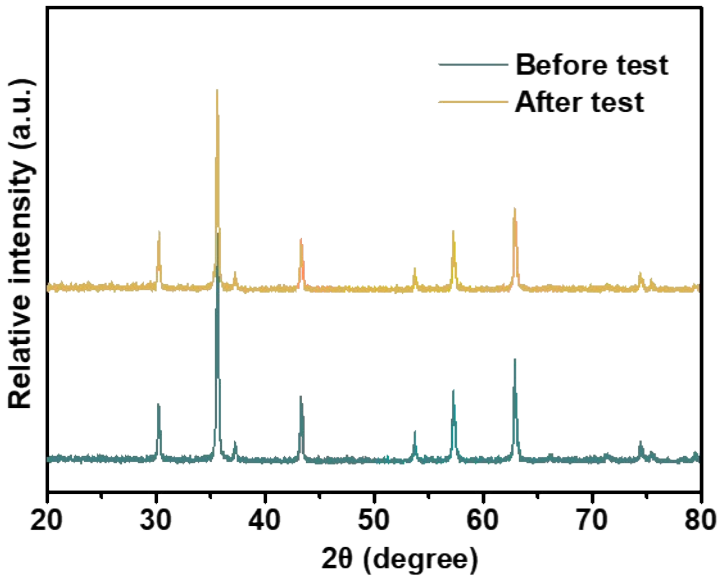

Fig. S4 XRD patterns of $NiFe_2O_4$ before and after testing.

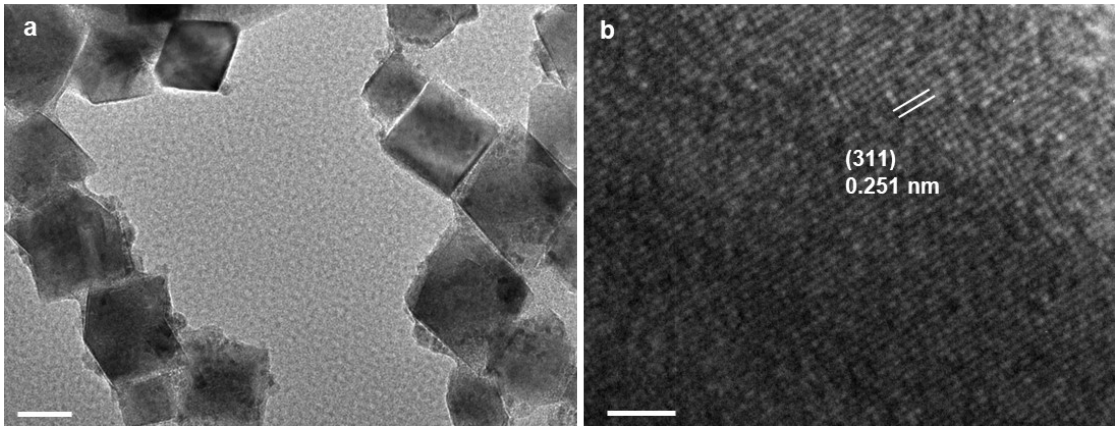

Fig. S5 TEM(a) and HRTEM(b) of $NiFe_2O_4$ after testing. Scale bars in TEM and HRTEM images represent 50 nm and 2 nm, respectively.

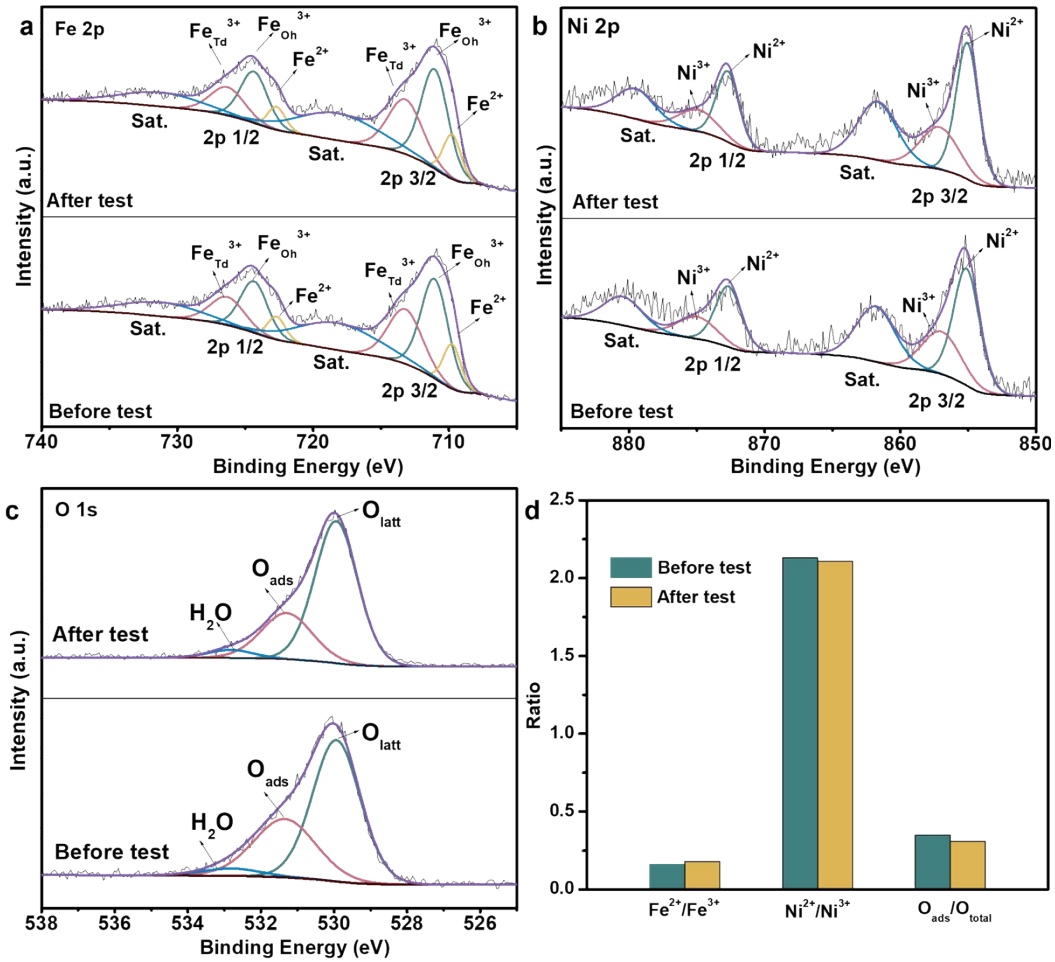

Fig. S6 (a) Fe 2p, (b) Ni 2p, (c) O 1s XPS spectra and (d) Quantitative analysis of different valence states of surface metals and different oxygen species for $NiFe_2O_4$ before and after testing.

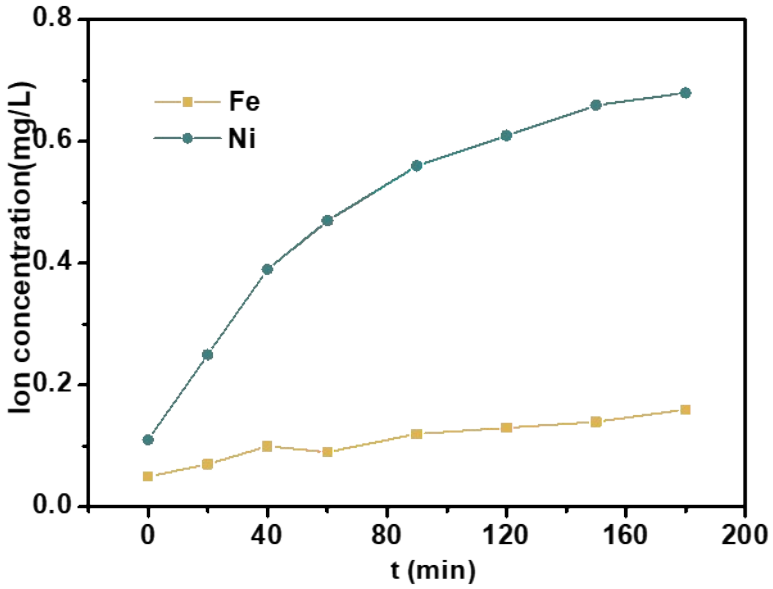

Fig. S7 The change of ion concentration with time in $NiFe_2O_4/H_2O_2$ system.

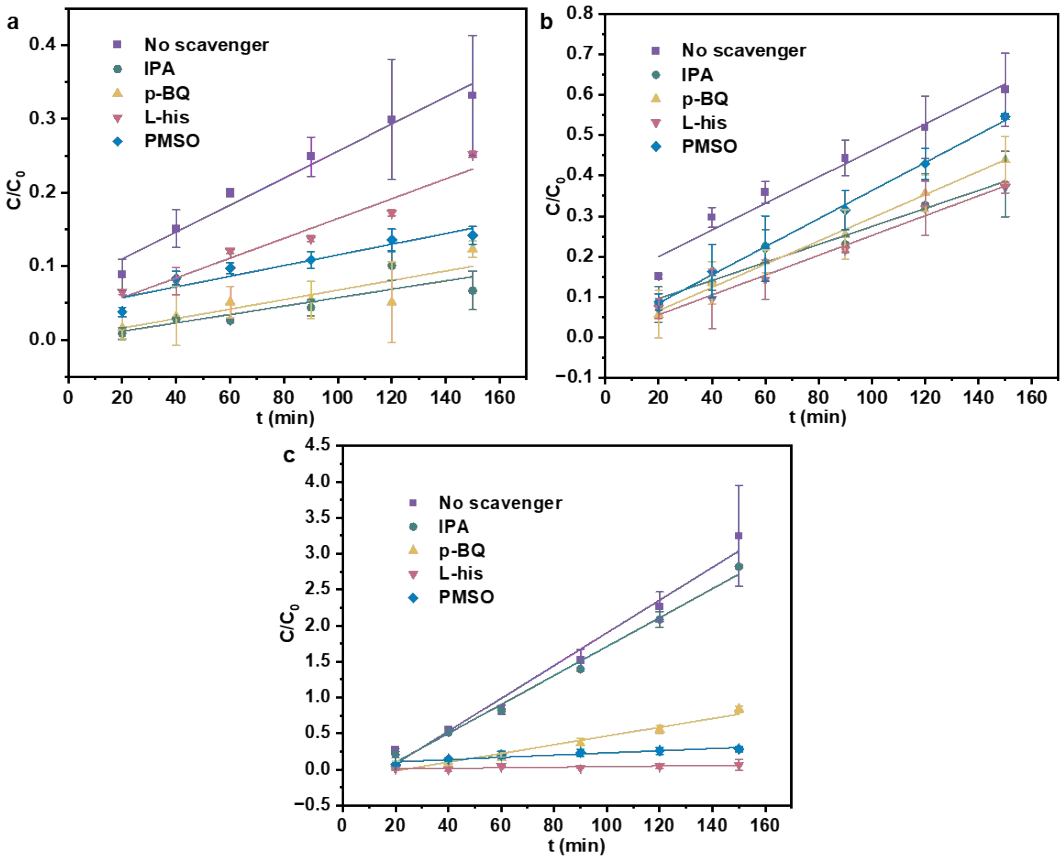

Fig. S8 The kinetic fitting results of (a) $CoFe_2O_4/H_2O_2$, (b) $Ni_{0.5}Co_{0.5}Fe_2O_4/H_2O_2$ and (c) $NiFe_2O_4/H_2O_2$ with various sacrificial reagents. For $CoFe_2O_4/H_2O_2$, the corresponding *k* value decreased from 0.0017 min^{-1} to ~0.0005 min^{-1} for the experiment with IPA and ~0.0006 min^{-1} for the experiment with *p*-BQ or PMSO as the scavengers; when *L*-his was used as the scavenger, the k value decreased to 0.0013 min^{-1}. The corresponding *k* value decreased from 0.00594 min^{-1} to 0.00367 min^{-1} for IPA, 0.00474 min^{-1} for *p*-BQ, to 0.00389 min^{-1} for *L*-his and to 0.00515 min^{-1} for PMSO in $Ni_{0.5}Co_{0.5}Fe_2O_4/H_2O_2$ system. In $NiFe_2O_4/H_2O_2$ system, the corresponding *k* value decreased from 0.0203 min^{-1} to 0.0202 $min^{-1}$for IPA, 0.0061 min^{-1} for *p*-BQ, to 0.0004 min^{-1} for *L*-his and to 0.0015 min^{-1} for PMSO.

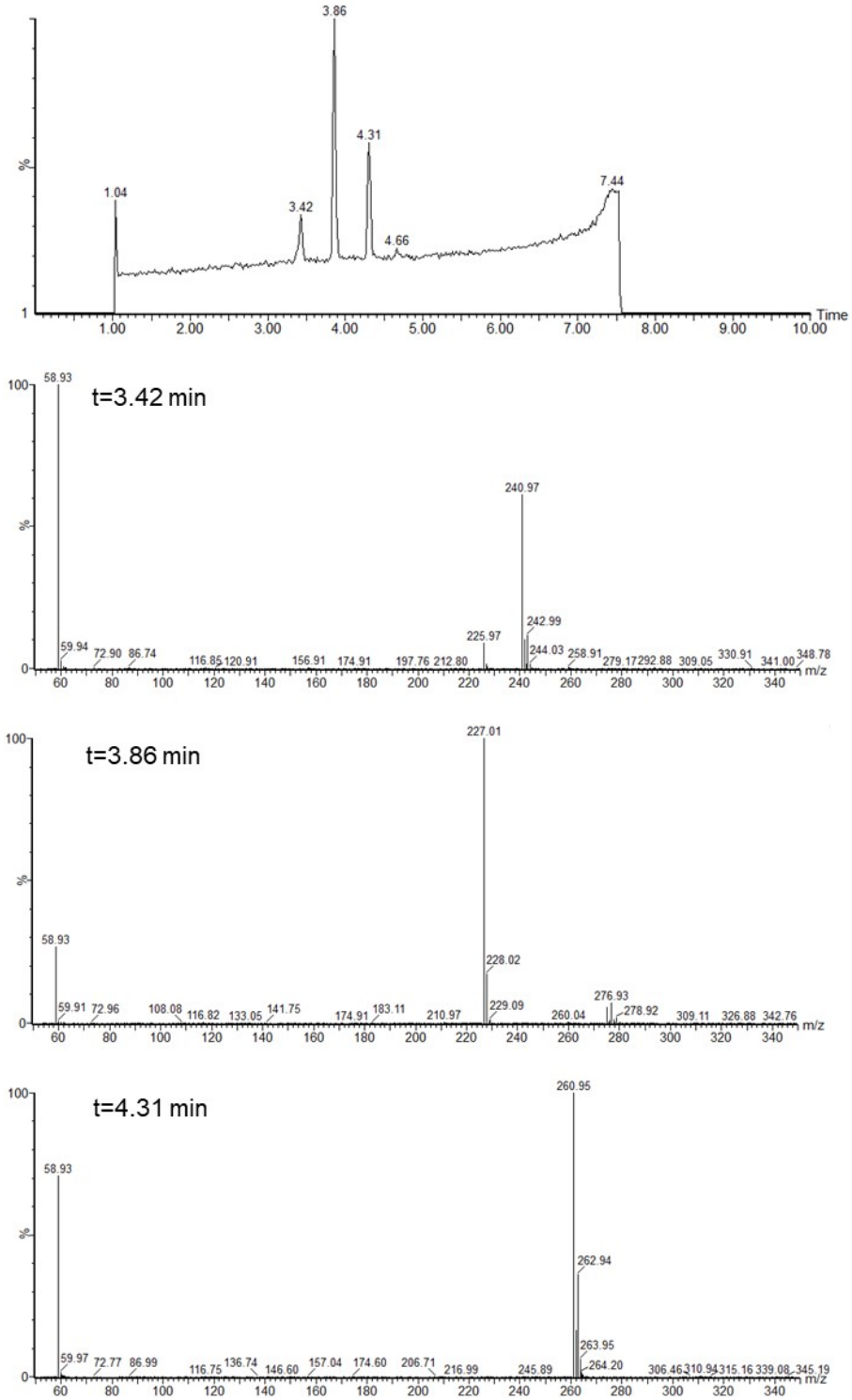

Fig. S9 HPLC-MS analysis of BPA degradation intermediates in $CoFe_2O_4/H_2O_2$.

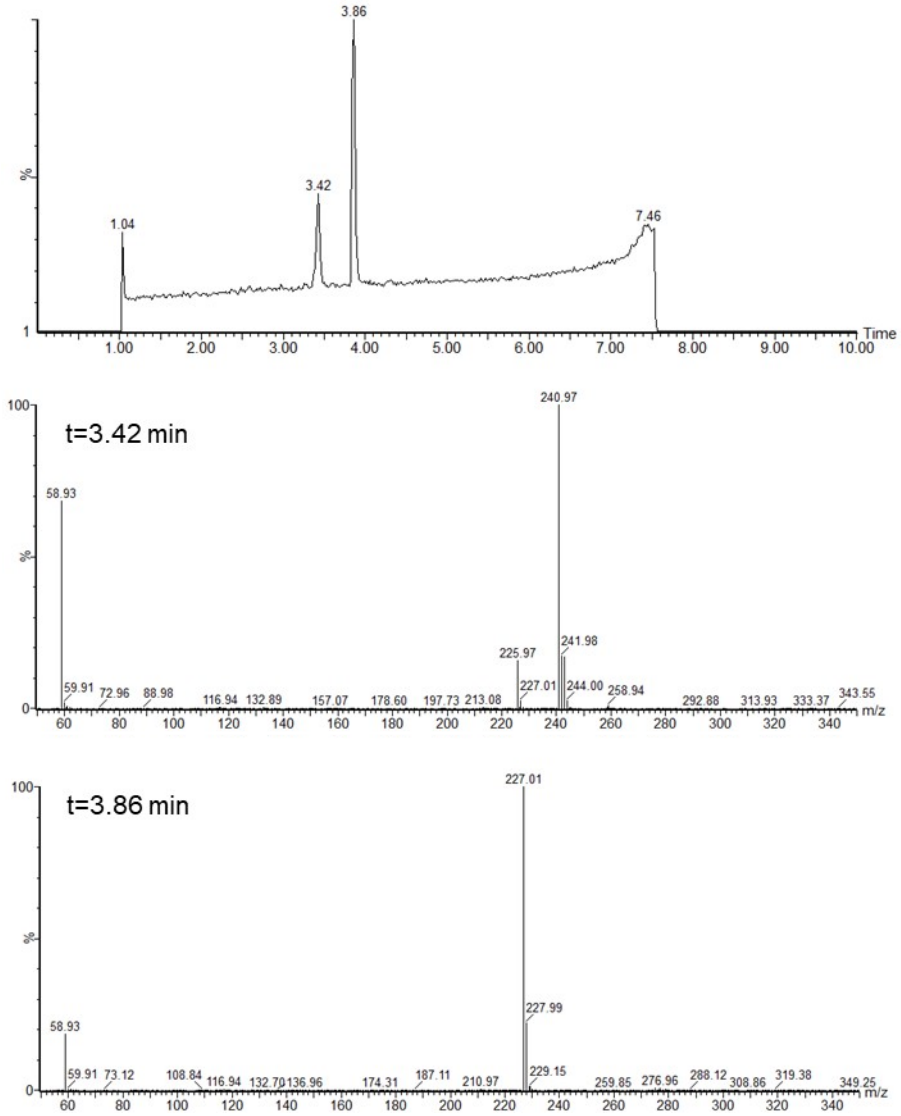

Fig. S10 HPLC-MS analysis of BPA degradation intermediates in $NiFe_2O_4/H_2O_2$.

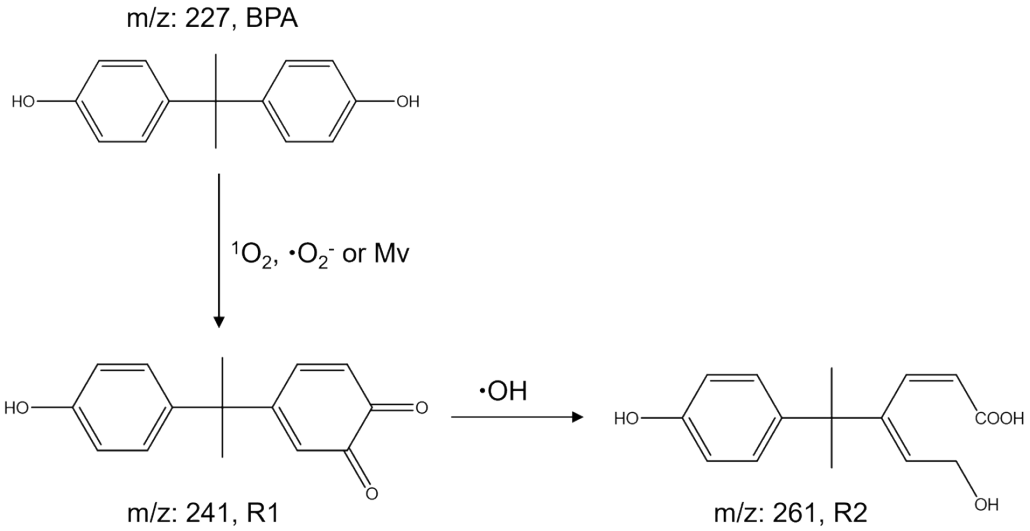

Fig. S11 Possible degradation pathways of BPA caused by active species.

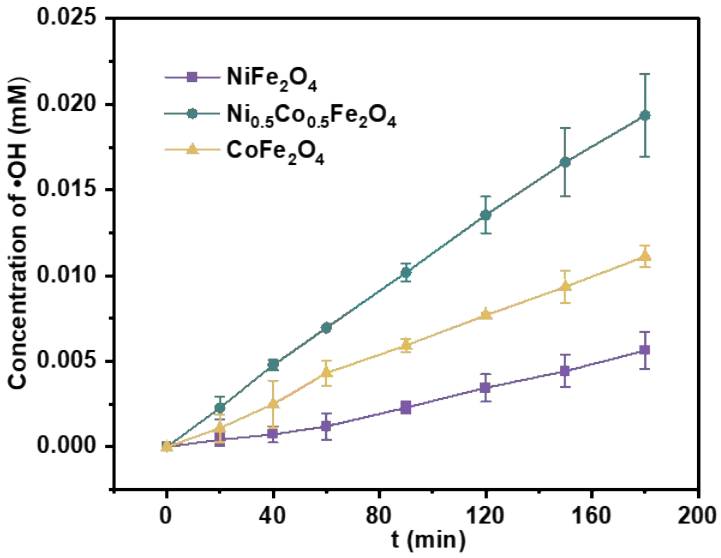

Fig. S12 Accumulated concentration of ·OH produced by $Ni_xCo_{1-x}Fe_2O_4/H_2O_2$. The yield of ·OH in these systems followed the order of $Ni_{0.5}Co_{0.5}Fe_2O_4/H_2O_2$ (0.019 ± 0.002 mM) > $CoFe_2O_4/H_2O_2$ (0.011 ± 0.001 mM) >$NiFe_2O_4/H_2O_2$ (0.006 ± 0.001 mM). For $^1O_2$, in spite of being the most efficient scavenger, FFA was able to intercept only 55 % of the $^1O_2$ generated, so the $Ni_{0.5}Co_{0.5}Fe_2O_4$ activated H_2O_2 produced less $^1O_2$ than that of $NiFe_2O_4$ (0.049 ± 0.015 mM vs. 0.175 ± 0.013 mM). The amount of ·OH produced was an order of magnitude lower than the amount of $^1O_2$ produced by $NiFe_2O_4/H_2O_2$. Thus, $NiFe_2O_4$ has higher catalytic efficacy in comparison to $Ni_{0.5}Co_{0.5}Fe_2O_4$ and $CoFe_2O_4$.

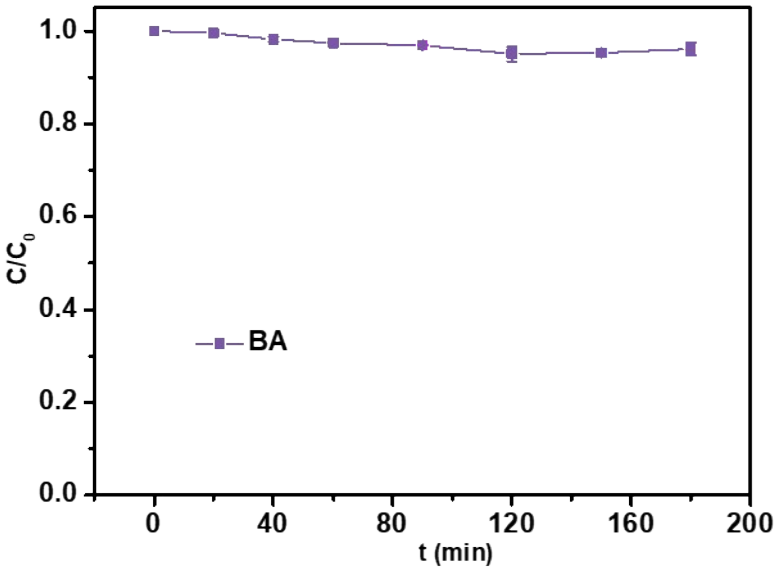

Fig. S13 Degradation of BA by $NiFe_2O_4/H_2O_2$ system. Reaction conditions: *c*(BA)= 0.1 mM, *c*($NiFe_2O_4$)= 2 g/L, *c*(H_2O_2)= 20 mM, pH= 3.0. BA is considered to be resistant to non-radical degradation. It can be seen that in the $NiFe_2O_4/H_2O_2$ system, BA hardly degrades, further proving that the degradation reaction is dominated by non-radical pathways.

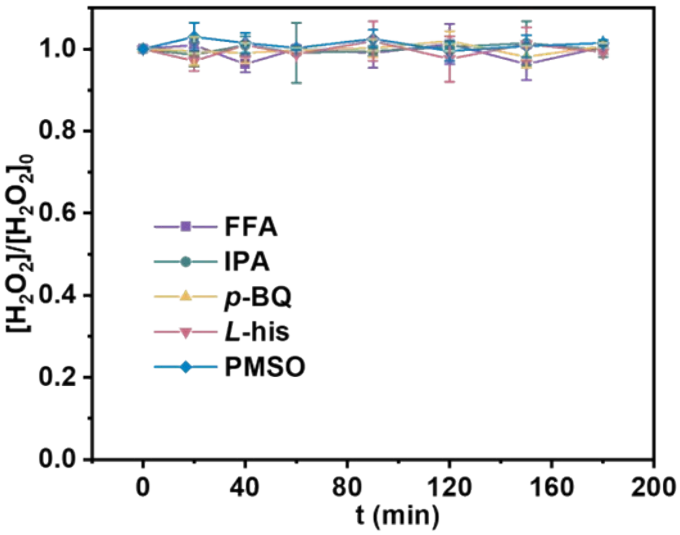

Fig. S14 Changes in H_2O_2 concentration in the presence of sacrificial agents.

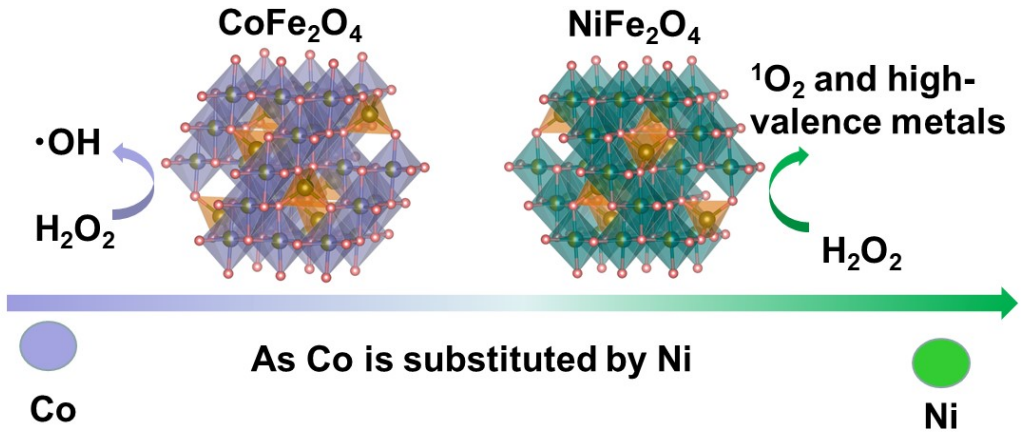

Fig. S15 Schematic diagram of the $CoFe_2O_4$ and $NiFe_2O_4$ activating H_2O_2 to produce active species.

Table S1. Detailed dosing amounts of precursors for different $Co_{1-x}Ni_xFe_2O_4$ (unit: g)

	$Co(NO_3)_3·6H_2O$	$Ni(NO_3)_3·6H_2O$	$Fe(NO_3)_3·9H_2O$
$CoFe_2O_4$	0.4366	0	1.2120
$Ni_{0.5}Co_{0.5}Fe_2O_4$	0.2183	0.2181	1.2120
$NiFe_2O_4$	0	0.4362	1.2120

Table S2. The ratio of metal ion with different electronic structure determined by XPS.

	$CoFe_2O_4$	**$Ni_{0.5}Co_{0.5}Fe_2O_4$**	**$NiFe_2O_4$**
Fe^{2+}/Fe^{3+}	0.17	0.17	0.15
$Fe_{Oh}^{3+}/Fe_{Td}^{3+}$	1.28	1.37	1.48
Ni^{2+}/Ni^{3+}	-	2.39	2.13
Co^{2+}/Co^{3+}	3.35	3.14	-
O_{ads}/O_{total}	0.23	0.36	0.37

Table S3. Comparison of degradation of BPA by Fe-based materials catalyzed Fenton-like systems.

Entry	Catalyst	Initial experimental condition	Degradation rate and time	Ref
1	Carbon nanotube-supported Fe_3O_4	[BPA]= 0.3 m M, [Cat.]= 1g/L, [H_2O_2]= 0.6 mM, pH 3	~70 % in 2 h	[11]
2	Fe_3O_4 magnetic nanoparticles	$[BPA]_0$= 20 mg/L, [Cat.]= 585 mg/L, [H_2O_2]= 160 mM, pH 3, Ultrasonic	~95% in 8 h	[12]
3	$CuFeO_2$ 1.0 g/L	[BPA]= 20 mM, [Cat.]= 1 g/L, [H_2O_2]= 1 mM, pH 5	~100% in 120 min	[13]
4	nZVI	[BPA]= 25 mg/L, [Cat.]= 0.2 g/L, [H_2O_2]= 20 mM, pH 5.75	~100% in 12 h	[14]
5	Goethite	$[BPA]_0$= 20 μM, [Cat.]= 0.1 g/L, [H_2O_2]= 1.13 mM, pH 6.2 UV	~10% in 360 min	[15]
6	Fe_3O_4/GO	[BPA]= 20 mg/L, [Cat.]= 1 g/L, [H_2O_2]= 10 mM, pH 2 or 6	~80% in 12 h in pH 6; ~90% in 10 h in pH 2	[16]
7	Graphitized carbon and nZVI	[BPA]= 25 μM, [Cat.]= 50 mg/L, [H_2O_2]= 0.5 mM, pH 6, UVA	~90% in 30 min	[17]
8	Magnetic illite clay-composite material	[BPA]= 80 mg/L, [Cat.]= 2 g/L, [H_2O_2]= 3 mM, pH 3	99.53% in 24 h	[18]
9	Nano-Fe_3O_4	[BPA]= 80 mg/L, [Cat.]= 2 g/L, [H_2O_2]= 3 mM, pH 3	99.42% in 24 h	[18]
10	α-FeOOH	[BPA]= 0.1 mM, [Cat.]= 0.5 g/L, [H_2O_2]= 1 mM, pH 4.5	75.9% in 240 min	[19]
11	Iron-carbon composites	BPA]= 20 mg/L, [Cat.]= 0.5 g/L, [H_2O_2]= 0.8 mM, pH 3.5	78% in 180 min	[20]

References

1. M. Qanbarzadeh, D. Wang, M. Ateia, S.P. Sahu, E. L. Cates, *ACS ES&T Eng.*, 2020, **1**, 239-248.
2. P. Hong, K. Zhang, J. He, Y. Li, Z. Wu, C. Xie, J. Liu, L. Kong, *J. Hazard. Mater.*, 2022, **435**, 128958.
3. H. Che, P. Wang, J. Chen, X. Gao, B. Liu, Y. Ao, *Appl. Cat., B*, 2022, **316**, 121611..
4. S. H. Joo, A. J. Feitz, D. L. Sedlak and T. D. Waite, *Environ. Sci. Technol.*, 2005, **39**, 1263-1268.
5. K. Mopper and X. Zhou, *Science (New York, N.Y.)*, 1990, **250**, 661-664.
6. Z. Zhou, Y. Zhang, Z. Wang, W. Wei, W. Tang, J. Shi and R. Xiong, *Appl. Surf. Sci.*, 2008, **254**, 6972-6975.
7. M. Li, Y. Mao, H. Yang, W. Li, C. Wang, P. Liu and Y. Tong, *New J. Chem.*, 2013, **37**, 3116-3120.
8. C. Solis, S. Somacescu, E. Palafox, M. Balaguer and J. M. Serra, *J. Phys. Chem. C*, 2014, **118**, 24266-24273.
9. Y. Jiang, Z. Geng, L. Yuan, Y. Sun, Y. Cong, K. Huang, L. Wang and W. Zhang, *ACS Sustainable Chem. Eng.*, 2018, **6**, 11999-12005.
10. M. J. Kang, H. Park, J. Jegal, S. Y. Hwang, Y. S. Kang and H. G. Cha, *Appl. Cat., B*, 2019, **242**, 85-91.
11. V. Cleveland, J.-P. Bingham and E. Kan, *Sep. Purif. Technol.*, 2014, **133**, 388-395.
12. R. Huang, Z. Fang, X. Yan and W. Cheng, *Chem. Eng. J.*, 2012, **197**, 242-249.
13. X. Zhang, Y. Ding, H. Tang, X. Han, L. Zhu and N. Wang, *Chem. Eng. J.*, 2014, **236**, 251-262.
14. L. Ma, H. He, R. Zhu, J. Zhu, I. D. R. Mackinnon and Y. Xi, *Catal. Sci. Technol.*, 2016, **6**, 6066-6075.
15. W. Huang, M. Brigante, F. Wu, K. Hanna and G. Mailhot, *Environ. Sci. Pollut. Res.*, 2013, **20**, 39-50.
16. Z. Hua, W. Ma, X. Bai, R. Feng, L. Yu, X. Zhang and Z. Dai, *Environ. Sci. Pollut. Res.*, 2014, **21**, 7737-7745.
17. M. Cai, J. Li, F. Wu, G. Voyard, G. Mailhot and M. Brigante, *J. Environ. Chem. Eng.*, 2023, **11**, 110959.
18. T. Bao, M. M. Damtie, W. Wei, H. N. P. Vo, K. H. Nguyen, A. Hosseinzadeh, K. Cho, Z. M. Yu, J. Jin, X. L. Wei, K. Wu, R. L. Frost and B.-J. Ni, *J. Clean. Prod.*, 2021, **287**, 125068.
19. J. Ding, L. Shen, R. Yan, S. Lu, Y. Zhang, X. Zhang and H. Zhang, *Chemosphere*, 2020, **261**, 127715.
20. Y. Chen, Y. Shi, D. Wan, Y. Liu, Y. Wang, X. Han and M. Liu, *Colloid. Surfaces A,* 2022, **639,** 128376.